Journal of Applied Mechanics and Technical Physics, Vol. 46, No. 6, pp. 800–806, 2005

EXPERIMENTAL STUDY OF THE DYNAMIC EFFECT OF AN INTERNAL SOLITARY WAVE ON A SUBMERGED CIRCULAR CYLINDER

E. V. Ermanyuk and N. V. Gavrilov

UDC 532.59

The hydrodynamic loads due to the interaction of a small-amplitude internal solitary wave with a submerged circular cylinder in a two-layer system of miscible fluids were studied experimentally. The dependence of the internal-wave transmission coefficient on the position of the center of the cylinder relative to the pycnocline and on the ratio of the cylinder diameter to the fluid-layer thickness was obtained. The effects of the pycnocline thickness and the depth of the center of the cylinder on the value of the hydrodynamic loads were studied. Visualization of the flow structure was performed.

Key words: *stratified fluid, internal solitary wave, hydrodynamic load.*

Introduction. The dynamic effect of free internal waves on submerged bodies can be estimated as a first approximation using linear wave theory [1–3]. Experimental studies of the interaction of periodic internal waves with submerged bodies under stratification conditions close to two-layer stratification are described in [4, 5]. However, full-scale data show that because of the shallow depth of the main thermocline in the ocean, internal waves propagate over it as a train of solitonlike perturbations [6], which have a marked dynamic effect on underwater vehicles and marine facilities [7]. The theory of internal solitary waves has been developed most fully for two-layer fluids with a density jump at the interface [8, 9]. More general cases of density distribution over depth are considered in [10–13]. Experimental studies of the parameters of internal solitary waves and their comparison with theoretical estimates for systems with a smoothly varying pycnocline are presented in [14, 15]. However, data on the dynamic effect of internal solitary waves on submerged obstacles are not available in the literature.

The present paper gives results from an experimental study of the interaction of an internal solitary wave with a submerged circular cylinder. Solitary waves were generated in the lower layer of a two-layer system of miscible fluids. The wave parameters were compared with their theoretical estimates [9] for a two-layer system with a density jump at the interface. Measurements were performed of the vertical and horizontal components of the hydrodynamic load and the propagation coefficient of the internal solitary wave as a function of the position of the cylinder relative to the pycnocline. Flow visualization showed that the interaction of the cylinder with the solitary wave led to the formation of high-gradient layers in the vicinity of the cylinder.

Experimental Procedure. The experiments were performed in a $400 \times 20 \times 15$ cm hydrodynamic tank filled with a stratified two-layer fluid (Fig. 1). The tank was first filled with the lower layer (a sugar solution in distilled water) of depth h_1 and density ρ_1 and then with the upper layer (distilled water) of depth h_2 and density ρ_2, which was slowly poured in through porous floats. Some time after the filling, the diffusion of sugar in the tank gave rise to a vertical density distribution $\rho(y)$. In a coordinate system attached to the free surface (the y axis is directed upward and the positive x direction coincides with the propagation direction of the solitary wave), this distribution was well approximated by the relation

$$\rho(y) = \rho_0 - (\varepsilon\rho_2/2)\tanh\,(2(y + h_2)/\delta), \tag{1}$$

Lavrent'ev Institute of Hydrodynamics, Siberian Division, Russian Academy of Sciences, Novosibirsk 630090; ermanyuk@hydro.nsc.ru. Translated from Prikladnaya Mekhanika i Tekhnicheskaya Fizika, Vol. 46, No. 6, pp. 36–44, November–December, 2005. Original article submitted January 21, 2005.

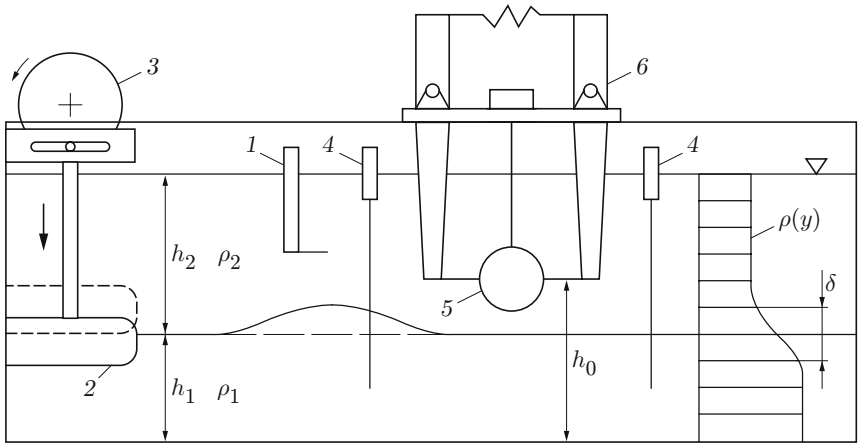

Fig. 1. Diagram of the experimental setup: 1) sensor; 2) wavemaker; 3) link mechanism; 4) wavemeters; 5) circular cylinder; 6) hydrodynamic balance.

where $\rho_0 = (\rho_1 + \rho_2)/2$ and $\varepsilon = (\rho_1 - \rho_2)/\rho_2$. The vertical density distribution was measured by a probe with horizontal sensitive elements. Because of the smallness of the sugar diffusion coefficient, the pycnocline thickness δ varied insignificantly during one series of experiments. Control measurements performed before and after the experiments showed that δ increased by not more than 0.2 cm.

Solitary waves were generated by a wavemaker in the form of a thick plate 20 cm long with rounded edges, which was moved by a link mechanism from its upper dead point to the lower one. In the initial position, the lower edge of the plate was at a distance h_1 from the bottom of the tank, and then was smoothly moved downward a distance A for a certain characteristic time T. The perturbation produced by the wavemaker became a hump-type solitary wave at a certain distance from it. With a proper choice of A and T, the dispersive wake behind the solitary wave was insignificant.

The waves were recorded by two resistance wavemeters with vertically arranged sensors. The wavemeters were at $l_1 = 100$ cm and $l_2 = 280$ cm from the wavemaker. The parameters of the incident, reflected, and transmitted waves were measured. It should be noted that the output signal of the wavemeters with vertical sensors is proportional to the vertical displacement of the fluid particles averaged over the pycnocline thickness with the weight function $d\rho/dy$ [16]. For a small pycnocline thickness and long internal waves, the output signal of the wavemeter served as a measure of the vertical displacement of the conventional interface (the equidensity line ρ_0). The dynamic characteristics of the wavemeter were determined from its response $R(t)$ to a stepwise displacement. The wavemeter is a linear system, and its response $w(t)$ to an arbitrary action $f(t)$ can be represented as the convolution $w(t) = \int\limits_0^\infty \Big(\frac{dR(\tau)}{d\tau}\Big) f(t-\tau)\, d\tau$. The test function $f(t)$ was chosen using the solution of [9] which describes the elevation of the interface of a two-layer fluid due to the passage of an internal wave with parameters close to experimental values. In the examined range of solitary-wave parameters, the waveform distortion was negligible, the signal lag with respect to the wave arrival time did not exceed 0.7 sec, and the wave amplitude was underestimated by 3%, which was taken into account in processing the experimental records.

The instantaneous hydrodynamic loads acting on the submerged circular cylinder of diameter D were measured using a hydrodynamic two-component balance. The center of the cylinder was at a distance h_0 from the bottom of the tank and at a distance of $l = (l_1 + l_2)/2$ from the wavemaker. The analog signals from the hydrodynamic load sensors and the wavemeters were processed with a computer furnished with a 12-bit analog-to-digital converter. The gravity-current pattern and its interaction with the submerged cylinder were photographed by a digital camera. Visualization was performed using the following technique [17]: a luminous screen with a grid of inclined lines drawn on it was photographed through the water layer. In zones with a high density gradient, a characteristic distortion of the lines was observed whose value, as a first approximation, is proportional to the local density gradient.

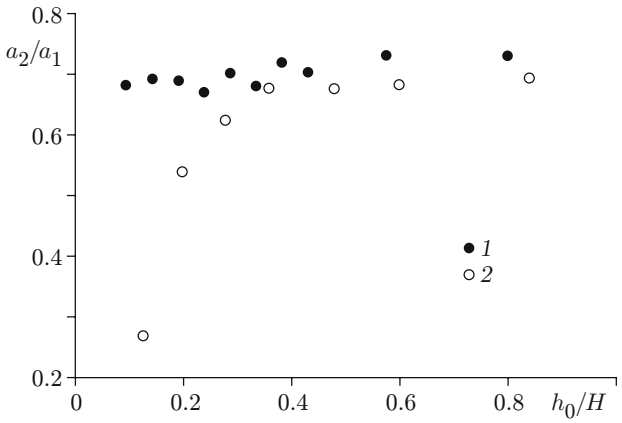

Fig. 2. Solitary-wave propagation coefficient versus the dimensionless distance between the center of the cylinder and the tank bottom. Points 1 and 2 correspond to the data obtained for $D = 1.5$ cm and 3 cm, respectively.

Experimental Results. A simple theoretical idealization of the smooth density distribution (1) is the model of an ideal two-layer fluid with an interface between the layers. A solution for solitary waves in an ideal two-layer fluid was first obtained by L. V. Ovsyannikov [8]. Funakoshi and Oikawa [9] obtained a solution which is close to that of [8] and has a form convenient for practical calculations. According to [9], for $\varepsilon \ll 1$, the profile of an internal solitary wave of amplitude a is given by the expression

$$\xi(x) = a\,\frac{\cosh^{-2}(kx/H)}{1-\theta\tanh^{2}(kx/H)}, \tag{2}$$

where ξ is reckoned from the unperturbed interface between the layers, a is the amplitude of the solitary wave, $k = 2\sqrt{3\eta_0(1-2\eta_\infty-\eta_0)}$, $\theta = \eta_0/(1-2\eta_\infty-\eta_0)$, $\eta_0 = a/H$, and $\eta_\infty = h_1/H$. The equation for the propagation velocity of the internal solitary wave is written as

$$V_0 = (1-2(\eta_0+\eta_\infty-0.5)^2)\sqrt{\varepsilon g H}\,/2 \tag{3}$$

(g is the acceleration of gravity). The variation in the free-surface level at a certain fixed point in space with time t is described by the expression (2) with the change of variable $x = x_1 - V_0 t$.

In the experiments, the amplitude a of the internal solitary waves was varied from 0.2 to 0.9 cm, and the characteristic pycnocline thickness δ from 1.5 to 3.9 cm. The average ratio of the experimental velocity V to the value of V_0 obtained from (3) was $V/V_0 = 0.85$ with an error of ± 1 %, which is in good agreement with [14]. In the examined range of experimental parameters, expression (2) adequately describes the time variation in the interface level with the change of variable $x = x_1 - Vt$, which agrees with the conclusions of [14, 15].

The damping of internal solitary waves due to friction on the bottom and walls of the tank and the intensity of reflection of internal waves from the submerged cylinder are described by the relation a_2/a_1, where a_1 and a_2 are the wave amplitudes measured by the first and second wavemeters, respectively. Measured values of a_2/a_1 versus h_0/H for $\delta = 2.8$ cm, $H = 12.5$ cm, and $h_1 = 4$ cm are given in Fig. 2 for $D = 1.5$ and 3 cm. For $D = 1.5$ cm, the cylinder has little effect on the propagation of the internal solitary wave. For this value of D, the characteristic values of the flow-blocking coefficients for the upper and lower fluid layers are $D/h_1 = 0.375$ and $D/h_2 = 0.176$ respectively. For all h_0/D, we have $a_2/a_1 \approx 0.7$. Control measurements performed in the absence of the cylinder gave the same value of a_2/a_1 within the experimental accuracy.

For $D = 3$ cm, the flow-blocking coefficient determined from the lower fluid layer approaches unity ($D/h_1 = 0.75$). Accordingly, for the cylinder located in the lower fluid layer, i.e., at $h_0 < h_1$ ($h_0/H < 0.32$), the ratio a_2/a_1 decreases sharply compared to the case of insignificant flow blocking. The internal-wave propagation coefficient a_2/a_1 has a minimum value when the cylinder is in the lower fluid layer at $h_0/D \to 0.5$. At $h_0/H > 0.32$, the cylinder is in the upper fluid layer and the results for a_2/a_1 obtained in the experiments for $D = 3$ and 1.5 cm almost coincide.

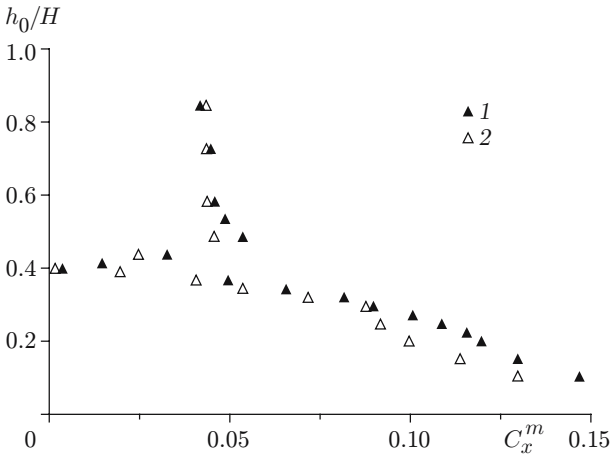

Fig. 3

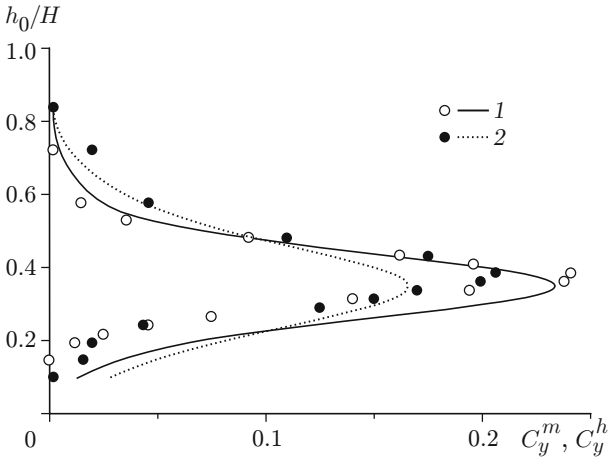

Fig. 4

Fig. 3. Amplitude of the horizontal-force coefficient C_x^m versus the dimensionless distance between the center of the cylinder and the tank bottom h_0/H (the data are obtained for $D = 1.5$ cm): points 1 refer to $\delta = 2.8$ cm and $a_c = 0.72$ cm and points 2 to $\delta = 3.9$ cm and $a_c = 0.68$ cm.

Fig. 4. Amplitude of the vertical-force coefficient C_y^m (points) and their quasihydrostatic estimates C_y^h (curves) versus the dimensionless distance between the center of the cylinder and the tank bottom h_0/H (the data were obtained for $D = 1.5$ cm): solid curve and points 1 refer to $\delta = 2.8$ cm and $a_c = 0.72$ cm, and dotted curve and points 2 refer to $\delta = 3.9$ cm and $a_c = 0.68$ cm.

Figures 3 and 4 show measured values of the maximum hydrodynamic loads for the horizontal and vertical forces, respectively. The hydrodynamic loads were measured for $H = 12.5$ cm, $h_1 = 4$ cm, and $\varepsilon = 0.021$ in two series of experiments: for $a = 0.72$ cm and $\delta = 2.8$ cm in the first series and $a = 0.68$ cm and $\delta = 3.9$ cm in the second series. The dimensionless hydrodynamic-load coefficients per unit length of the cylinder are given by the expressions

$$C_{x,y} = F_{x,y}/(\varepsilon\rho_2 g S), \tag{4}$$

where S is the cross-sectional area of the cylinder. By the amplitudes of the hydrodynamic coefficients $C_{x,y}^m$ we mean the moduli of their maximum values in each series of experiments: $C_{x,y}^m = \max|C_{x,y}(t)|$. As one might expect, the horizontal load is maximum when the cylinder lies on the bottom ($h_0/D \to 0.5$), and it is nearly zero for $h_0 \approx h_1 + a$. The minimization of C_x^m for $h_0 \approx h_1 + a$ is due to the existence of a tangential velocity discontinuity at the interface between the upper and lower fluids. For $h_0/H > 0.6$, the value of C_x^m is approximately constant. In this case, the cylinder is completely in the upper fluid layer and the flow blocking in the upper fluid layer is insignificant. The constancy of C_x in this case confirms the conventional assumption of shallow water theory that the vertical distribution of the horizontal components of the fluid particle velocities can be considered uniform. This assumption is confirmed by direct measurements [15]. Generally, it should be noted that the values of C_x^m measured in both series of experiments are fairly close although with the nearly unchanged wave amplitude, the characteristic pycnocline thickness varied significantly: from 2.8 cm in the first series of experiments to 3.9 cm in the second series. This suggests that the horizontal momentum of internal solitary waves and the horizontal velocities and accelerations of fluid particles in a stratified fluid with a density distribution of the form of (1) should depend weakly on δ.

The vertical-force coefficient C_y^m is maximum when the cylinder is in the pycnocline (see Fig. 4). The vertical hydrostatic load was estimated under the assumption that the cylinder disturbs the density field only slightly and that the time variations of the density field are obtained from (1) by the substitution $h_2 = h_2 - \xi(t)$. The maximum vertical load C_y^h estimated using the above-mentioned assumptions are shown in Fig. 4 by dotted and solid curves. It is evident that the quasihydrostatic approach underestimates the maximum values of the vertical-load amplitudes for the cylinder located in the central region of the pycnocline (at $h_0 \approx h_1 + a$) and overestimates the vertical-load amplitudes for the cylinder located in the lower fluid layer and partly submerged in the pycnocline.

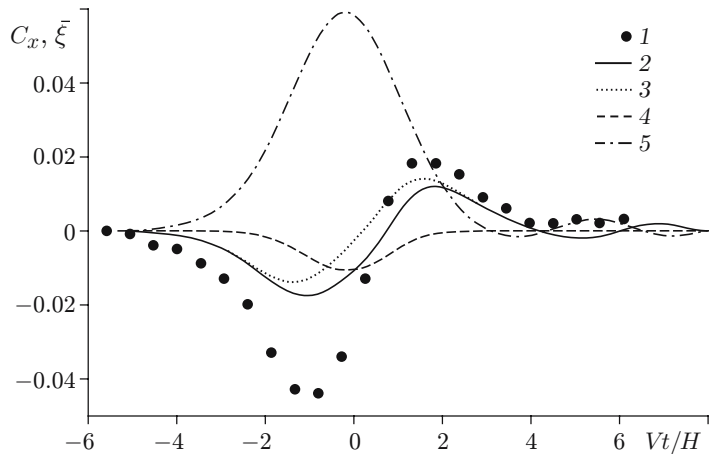

Fig. 5. Horizontal-force coefficient C_x versus dimensionless time for the cylinder located in the upper fluid layer: points 1 are experimental data; curve 2 is the estimate using Eq. (5); curves 3 and 4 are the inertial and damping components, respectively; curve 5 are the fluctuations of the interface level $\bar{\xi}$.

From the hydrostatic laws, it follows that in the limiting case $a \ll D$, $D < \delta$, the maximum scale of the variable buoyancy force C_y^h using the normalization (4) is equal to a/δ, and for $a \ll D$ and $\delta \ll D$, we have $4a/(\pi D)$. The conditions of the experiments corresponded to the first case.

For the cylinder located in the upper fluid layer, at $h_0/H > 0.6$, the hydrodynamic load can be estimated from the kinematic parameters of motion of fluid particles in the wave using the Morison equation [18]. According to the Morison equation, the horizontal hydrodynamic load is represented as the sum of the inertial and damping forces:

$$F_x(t) = C_x^{\text{in}} \rho S \frac{\partial u_x}{\partial t} + \frac{1}{2} C_x^{\text{d}} \rho D u_x |u_x|, \tag{5}$$

where u_x is the horizontal velocity component of fluid particles in the wave, C_x^{in} is the inertial coefficient, and C_x^{d} is the damping coefficient. The horizontal velocity component of fluid particles in the upper fluid layer can be estimated as $u_x = -V\xi(t)/h_2$. Direct measurements of [14, 15] showed that this estimate holds with good accuracy for small-amplitude solitary waves for moderate values of h_2/h_1. At $h_0/H > 0.6$, the cylinder weakly distorts the profile of the incident solitary wave. The velocity u_x and the local acceleration $\partial u_x/\partial t$ of fluid particles was estimated using the wave profile written at the point of measurement of hydrodynamic loads in the absence of the cylinder. Figure 5 gives the wave profile $\bar{\xi}(\tau) = \xi(\tau)/H$ (here $\tau = Vt/H$), experimental data for $C_x(\tau)$, the estimate of $C_x(\tau)$ calculated from the Morison equation, and the inertial and damping load components for the following combination of problem parameters: $h_1 = 4$ cm, $h_2 = 8.5$ cm, $\varepsilon = 0.021$, $a = 0.77$ cm, $h_0 = 9.5$ cm, and $\delta = 2.8$ cm. The propagation velocity of the solitary wave was $V = 6.79$ cm/sec. At $h_0 = 9.5$ cm, the cylinder is away from the bottom, the free surface, and the interface, so that we can set $C_x^{\text{in}} \approx 2$. The maximum value of the Reynolds number defined as $\text{Re} = Du_x^m/\nu$ (ν is the kinematic viscosity and $u_x^m = |-Va/h_2|$ is the maximum velocity of fluid particles in the upper layer) is $\text{Re} = 92$. For this Reynolds number, the drag coefficient for stationary flow over the cylinder (see, for example, the data of [19]) is $C_x^{\text{d}} \approx 1.5$. From Fig. 5, it is evident that for the above-mentioned values of the hydrodynamic-load coefficients, calculations using Eq. (5) greatly underestimate $C_x(t)$ compared to the experimental data. In particular, the maximum load is underestimated by a factor of approximately 2.5. The reason for this is that the Morison equation does not contain a term that takes into account the memory effect. For a sphere, the importance of taking into account the history force for $\text{Re} \approx 100$ can be shown using the Boussinesq solution. Some of latest experimental studies of the memory effect for a sphere moving in a viscous fluid, a review of the literature, and a discussion of the Boussinesq solution are presented in [20]. However, in the two-dimensional problem, a solution similar to the Boussinesq solution is difficult to obtain for the same reasons for which a finite value for the hydrodynamic drag of a circular cylinder at small Reynolds numbers is obtained only in the Oseen approximation [21]. We note that for large Reynolds numbers, which are typical of full-scale flows, one might expect improved accuracy of estimates of the type of (5).

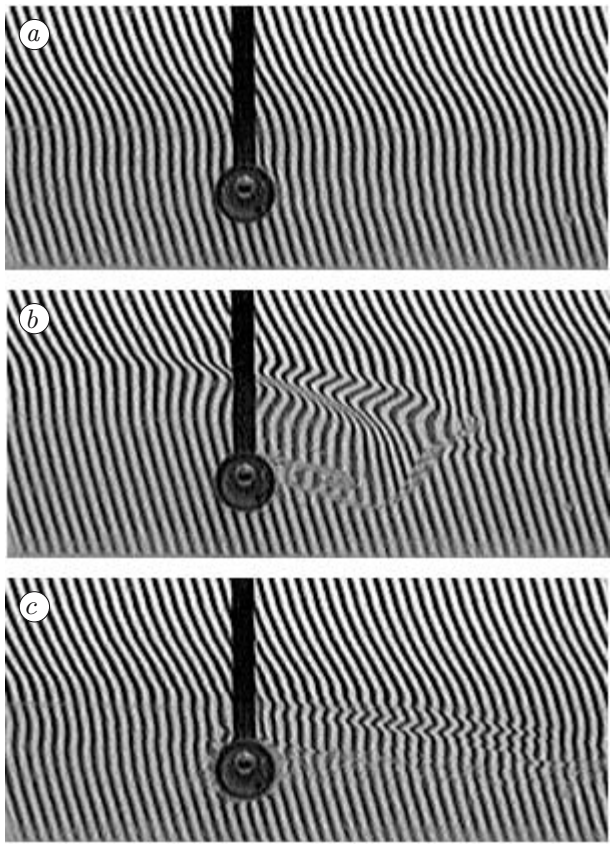

Fig. 6. Flow pattern in the vicinity of the cylinder located in the lower fluid layer at various times ($h_1 = 4$ cm, $H = 12.5$ cm, $h_0 = 2$ cm, and $\delta = 2.8$ cm): before the passage of the wave (a), after the passage of the wave crest (b), and after the passage of the wave (c).

An example of flow visualization in the vicinity of the cylinder is given in Fig. 6. It is evident that after the passage of the solitary wave, a stratification fine structure is formed in the vicinity of the cylinder; in these structure, the high-gradient layers are both attached (connected to the flow separation from the surface of the cylinder) and suspended (without origin on the solid surface). The suspended layers formed during uniform horizontal motion of two-dimensional obstacles in a linearly stratified fluid have been extensively studied (see, e.g. [22]). In the present paper, it is shown that suspended high-gradient layers can be formed during the interaction of internal solitary waves with obstacles in a continuously stratified fluid. In nature, a similar mechanism of formation of a stratification fine structure can be manifested during the interaction of internal solitary waves with bottom roughness.

Conclusions. The hydrodynamic loads exerted on a submerged circular cylinder by an internal solitary wave propagating in the lower layer of a two-layer system of miscible fluids were studied. It was shown that the horizontal load is maximum for the cylinder located on the channel bottom and is minimum for the cylinder near the interface. If the amplitude of the solitary wave does not change, the value of the horizontal load depends weakly on the pycnocline thickness. The vertical hydrodynamic load acting on the cylinder located in the pycnocline differs markedly from the estimate made on the basis of hydrostatics. Flow visualization showed that when an internal solitary wave is incident on the circular cylinder, a stratification fine structure in the form of a system of high-gradient layers occurs in the vicinity of the cylinder.

This work was supported by the Russian Foundation for Basic Research (Grant No. 04-01-00040) and Integration Project No. 3.13.1 of the Siberian Division of the Russian Academy of Sciences.

REFERENCES

1. I. V. Sturova, "Planar problem of hydrodynamic rolling of a submerged body at rest in a two-layer fluid," *Izv. Ross. Akad. Nauk, Mekh. Zhidk. Gaza*, No. 3, 670–679 (1994).
2. I. V. Sturova, "Planar problem of hydrodynamic rolling of a submerged body in the presence of motion in a two-layer fluid," *J. Appl. Mech. Tech. Phys.*, **35**, No. 5, 32–44 (1994).
3. T. I. Khabakhpasheva, "Diffraction of internal waves by a cylinder in a two-layer fluid," *Izv. Ross. Akad. Nauk, Fiz. Atmos. Okeana*, **29**, No. 4, 559–564 (1993).
4. E. V. Ermanyuk, "Experimental study of the force of internal waves acting on a stationary sphere," *J. Appl. Mech. Tech. Phys.*, **34**, No. 4, 543–546 (1993).
5. N. V. Gavrilov and E. V. Ermanyuk, "Effect of a pycnocline on the forces exerted by internal waves on a stationary elliptic cylinder," *J. Appl. Mech. Tech. Phys.*, **37**, No. 6, 825–833 (1996).
6. O. M. Phillips, *The Dynamics of the Upper Ocean*, Cambridge University Press, Cambridge (1966).
7. A. R. Osborne, T. L. Burch, and R. I. Scarlet, "The influence of internal waves on deep-water drilling," *J. Petrol. Technol.*, 1497–1504 (1978).
8. L. V. Ovsyannikov, N. I. Makarenko, V. I. Nalimov, et al., *Nonlinear Problems in the Theory of Surface and Internal Waves* [in Russian], Nauka, Novosibirsk (1985).
9. M. Funakoshi and M. Oikawa, "Long internal waves of large amplitude in a two-layer fluid," *J. Phys. Soc. Japan*, **55**, No. 1, 128–144 (1986).
10. T. B. Benjamin, "Internal waves of finite amplitude and permanent form," *J. Fluid Mech.*, **25**, 241–270 (1966).
11. D. J. Benney and D. R. S. Ko, "The propagation of long large amplitude internal waves," *Stud. Appl. Mech.*, **59**, 187–199 (1978).
12. N. I. Makarenko "Conjugate flows and smooth bores in a weakly stratified fluid," *J. Appl. Mech. Tech. Phys.*, **40**, No. 2, 69–78 (1999).
13. J. L. Maltseva, "Limiting forms of internal solitary waves," *J. Offshore Mech. Arctic Eng.*, **125(1)**, 76–79 (2003).
14. T. W. Kao, F.-S. Pan, and D. Renouard, "Internal solitons on the pycnocline: generation, propagation, and shoaling and breaking over a slope," *J. Fluid Mech.*, **159**, 19–53 (1985).
15. J. Grue, A. Jensen, P.-O. Rusas, and J. K. Sveen, "Properties of large amplitude internal waves," *J. Fluid Mech.*, **380**, 257–278 (1999).
16. N. V. Gavrilov and E. V. Ermanyuk, "Diffraction of internal waves by a circular cylinder near the pycnocline," *J. Appl. Mech. Tech. Phys.*, **40**, No. 2. 258–264 (1999).
17. V. I. Bukreev and N. V. Gavrilov, "Perturbations ahead of a wing moving in a stratified fluid," *J. Appl. Mech. Tech. Phys.*, No. 2, 102–105 (1990).
18. M. J. Lighthill, "Fundamentals concerning wave loading on offshore structures," *J. Fluid Mech.*, **173**, 667–682 (1986).
19. H. Schlichting, *Boundary Layer Theory*, McGraw-Hill, New York, (1968).
20. M. Abbad and M. Souhar, "Effects of the history force on an oscillating rigid sphere," *Exp. Fluids*, **36**, 775–782 (2004).
21. G. Birkhoff, *Hydrodynamics*, Princeton University Press, Princeton (1960).
22. V. V. Mitkin and Yu. D. Chashechkin, "Suspended discontinuities in the field of two-dimensional internal waves," *J. Appl. Mech. Tech. Phys.*, **40**, No. 5, 811–821 (1999).